

Journal Pre-proof



Stemless Reverse Neck-Shaft Angle Influences Humeral Component Time-Zero Fixation and Survivorship: A Cadaveric Biomechanical Assessment

David E. Cunningham, BEng, Ahmed A. Habis, MD, MSc, FRCSC, Fares Z.N. Uddin, MD, MRCSI, SB-ORTH, James A. Johnson, PhD, George S. Athwal, MD, FRCSC

PII: S2666-6383(24)00106-3

DOI: <https://doi.org/10.1016/j.jseint.2024.04.001>

Reference: JSEINT 992

To appear in: *JSES International*

Received Date: 28 March 2024

Accepted Date: 1 April 2024

Please cite this article as: Cunningham DE, Habis AA, Uddin FZN, Johnson JA, Athwal GS, Stemless Reverse Neck-Shaft Angle Influences Humeral Component Time-Zero Fixation and Survivorship: A Cadaveric Biomechanical Assessment, *JSES International* (2024), doi: <https://doi.org/10.1016/j.jseint.2024.04.001>.

This is a PDF file of an article that has undergone enhancements after acceptance, such as the addition of a cover page and metadata, and formatting for readability, but it is not yet the definitive version of record. This version will undergo additional copyediting, typesetting and review before it is published in its final form, but we are providing this version to give early visibility of the article. Please note that, during the production process, errors may be discovered which could affect the content, and all legal disclaimers that apply to the journal pertain.

© 2024 The Author(s). Published by Elsevier Inc. on behalf of American Shoulder and Elbow Surgeons.

Stemless Reverse Neck-Shaft Angle Influences Humeral Component Time-Zero Fixation and Survivorship: A Cadaveric Biomechanical Assessment

David E. Cunningham, BEng^{a,b}, Ahmed A. Habis, MD, MSc, FRCSC^{c,b,d}, Fares Z. N.

Uddin, MD, MRCSI, SB-ORTH^{e,b,d}, James A. Johnson, PhD^{a,b,d,f}, George S. Athwal, MD, FRCSC^{b,d,*}

^A Department of Mechanical Engineering, The University of Western Ontario, London, ON, Canada

^B The Roth|McFarlane Hand and Upper Limb Centre, St. Joseph's Hospital, London, ON, Canada

^C Department of Orthopaedic Surgery, Faculty of Medicine, King Abdulaziz University, Jeddah, Saudi Arabia.

^D Department of Surgery, The University of Western Ontario, London, ON, Canada

^e Bahrain Royal Guard / King Hamad University Hospital, Royal Medical Services - Bahrain Defence Force, Al Sayh, Bahrain

^f Department of Biomedical Engineering, The University of Western Ontario, London, ON, Canada

Corresponding Author: George S. Athwal MD, FRCSC gsathwal@hotmail.com

Roth | McFarlane Hand & Upper Limb Centre, London, ON, Canada

268 Grosvenor Street., London, ON, Canada

Disclaimers:

Funding: Implants donated by Stryker. No company had any input in to the experimentation, results, analysis or manuscript preparation.

George S. Athwal is a consultant for Stryker, Conmed, and Exactech, and has received research support from Stryker.

The other authors their immediate families, and any research foundations with which they are

affiliated have not received any financial payments or other benefits from any commercial entity related to the subject of this article.

Investigations performed at the Roth|McFarlane Hand and Upper Limb Center, London, Ontario, Canada

Institutional review board approval was not required for this study.

1 **Stemless Reverse Shoulder Arthroplasty Neck-Shaft Angle Influences Humeral Component**

2 **Time-Zero Fixation and Survivorship: A Cadaveric Biomechanical Assessment**

3 **Abstract:**

4 **Background:** Stemless humeral components are being clinically investigated for reverse shoulder
5 arthroplasty (RSA) procedures. There is, however, a paucity of basic science literature on the
6 surgical parameters that influence the success of these procedures. Therefore, this cadaveric
7 biomechanical study evaluated the neck shaft angle (NSA) of implantation on the survivability
8 and performance of stemless RSA humeral components during cyclical loading.

9 **Methods:** Twelve paired cadaveric humeri were implanted with stemless RSA humeral
10 components at NSAs of 135° and 145°. Implant-bone motion at the periphery of the implant was
11 measured with three optical machine vision USB3 cameras outfitted with c-mount premium lenses
12 and quantified with ProAnalyst® software. A custom three-dimensional loading apparatus was
13 used to cyclically apply three loading directions representative of physiological states at five
14 progressively increasing loading magnitudes. Stemless 135° and 145° implants were compared
15 based on the maximum implant-bone relative distraction detected, as well as the survivorship of
16 the implants throughout the loading protocol.

17 **Results:** Primary fixation and implant biomechanical survivorship were substantially better in the
18 145° NSA implants. The 135° NSA implants elicited significantly higher implant-bone distractions
19 during cyclical loading ($P = 0.001$), and implant survivorship was considerably lower in the 135°
20 NSA specimens when compared to the 145° NSA specimens (135° NSA: 0%, 145° NSA: 50%) (P
21 < 0.001).

22 **Conclusions:** Neck shaft angle is a modifiable parameter that influences time-zero implant
23 stability, as well as the early survivorship of the stemless RSA humeral components tested in this

24 study. Neck shaft angle resections of 145° appear to promote better stability than those utilizing
25 135° neck shaft angles during early postoperative eccentric loads. Further studies are required to
26 assess if other stemless reversed humeral implant designs have improved time-zero fixation at
27 higher neck-shaft angles.

28 **Level of evidence:** Basic Science Study; Biomechanics

29 **Keywords:** stemless; neck shaft angle; arthroplasty; implant design; reverse shoulder arthroplasty;
30 cuff tear arthropathy; implant micromotion

31 In recent years, stemless RSA humeral prostheses have been introduced to preserve healthy bone
32 stock, to minimize periprosthetic humeral fractures, and to simplify future revision surgeries^{9,17}.

33 Additionally, these shorter humeral implants have been shown to better-mimic the natural force-
34 transmission properties of the shoulder joint, thereby reducing risk of stress shielding in
35 periprosthetic bone¹⁸. However, stemless humeral implants rely primarily on metaphyseal bone
36 press-fit for stability and fixation, and are therefore vulnerable to poor initial fixation or loosening
37 depending on implantation and/or metaphyseal bone properties and morphology¹⁷, which often
38 may be compromised by disuse osteopenia or osteoporosis⁵.

39

40 Surgeons must decide on the surgical variable of resection inclination (or neck shaft angle) of the
41 humeral head. Currently, most standard RSA systems vary the NSA between 135° to 155°.
42 Previously, it has been reported that decreasing NSA may reduce the risk of scapular notching¹³,
43 and may increase total impingement-free range of motion¹³. With respect to implant fixation, a
44 recent computational finite element study reported that decreasing NSA may also significantly
45 decrease the initial fixation of stemless RSA humeral components, potentially leading to increased
46 incidence of premature failure in these implants⁵. This was commensurate to the results of a

47 previous retrospective clinical study, which found that in a small series RSA humeral component
48 loosening was more prevalent in 135° NSA stemmed implants when compared to 155° NSA
49 stemmed implants¹²; although the data was not statistically significant due to the small numbers.
50 As present, there is little clinical data available on failure modes of stemless RSA implants.

51

52 Currently, no in-vitro studies are available that have evaluated the effect of NSA in stemless RSA
53 humeral components during physiological loading. This present investigation compared 135° and
54 145° NSA stemless RSA humeral component performance and its effect on primary implant
55 stability and early survivorship. We hypothesized that humeral components implanted at 145° NSA
56 would exhibit better primary biomechanical stability and improved implant survivorship when
57 compared to those implanted at 135° NSA.

58 **Methods**

59 *Specimen Preparation:*

60 Twelve paired cadaveric shoulder specimens (height: 171 ± 4 cm, weight: 57 ± 20 kg) aged $57 \pm$
61 12 years (mean \pm standard deviation) were implanted with metaphyseal filling two-tiered round
62 stemless RSA humeral components (Tornier Perform® Stemless Reverse Humeral System, Stryker,
63 Kalamazoo, MI, USA) by three board-certified orthopedic surgeons (GSA, AH, FU). The implant
64 evaluated was of press-fit design, with a combination of 3D printed and plasma sprayed titanium
65 surface finishes. Nominal barrel and fin interferences of 1.5 mm and 0.75 mm were present,
66 respectively. The bone mineral density (BMD) of the local periprosthetic bone was calculated
67 using a clinical CT Scanner (GE 750HD Discovery Scanner; GE Healthcare, Chicago, IL, USA)

68 and cortical bone surrogate (SB3 model 450; GAMMEX, Middleton, WI, USA) and distilled water
69 phantoms. The average periprosthetic BMD of the specimens evaluated was $0.106 \pm 0.003 \text{ g/mm}^3$.

70

71 Each bilateral specimen pair (L/R) was randomized to receive a 135° NSA and a 145° NSA
72 implantation, and a single surgeon positioned both components in each pair. Each neck shaft angle
73 cut was prepared using an intramedullary diaphyseal referencing cut-guide (*Figure 1*). Two
74 stemless reverse humeral implant sizes were utilized, sized based on individual patient geometry.
75 A constant size was utilized between each bilateral $135^\circ/145^\circ$ NSA pair to remove the independent
76 variable of sizing. After the humeral head resection, the metaphyseal bone was reamed with an
77 appropriately sized reamer, followed by insertion of the stemless trial implant. After which, the
78 trial implant was removed, and the final implant was impacted in and press-fit into the prepared
79 humerus.

80 ***In-Vitro Loading Protocol:***

81 A custom loading apparatus (Figure 2) was used to apply three loading conditions representative
82 of aggressive boundary loading (extreme physiological loads) that a humeral implant might
83 reasonably experience in the early postoperative period. This boundary loading envelope was
84 calculated to represent the 95% percentile of all the relevant loads from instrumented humeral
85 implants that were available on the OrthoLoad database⁶ (Figure 3) – a database with records of
86 the articular forces generated from telemetized humeral implants during common upper limb
87 motions. This envelope was developed by plotting all relevant articular load vectors into the
88 humeral coordinate system, then establishing limits based on the upper and lower values ± 2
89 standard deviations from the mean in a spherical coordinate system.

90

91 Loads with vectors pointed most superior-inferiorly were predominantly 90° abduction motions,
92 whereas loads with vectors pointed most anterior-posteriorly included steering a steering wheel or
93 arm elevation motions. Most OrthoLoad⁶ loads were directed along the anterosuperior -
94 posteroinferior vector direction. These included combing hair, 2 kg waist-height lifting, and some
95 elevation and abduction motions⁶. Loads with the largest magnitude/eccentricity combination, and
96 therefore most challenging to implant fixation, included a 2 kg head-height lifting motion, a single
97 hand steering motion, and an unweighted 90-degree abduction motion. The aforementioned
98 boundary loads were reconverted into the humeral coordinate system for load application (Figure
99 4). For each trial, the order of loading direction was randomized. Each loading set (Superior,
100 Anterosuperior, and Anterior) was applied for 30 cycles at a frequency of 1 Hz at 20%, 40%, 60%,
101 80%, and 100% of the physiological magnitude.

102 ***Measurement of Implant Stability:***

103 Implant-bone micromotion (i.e. implant distraction orthogonal to the bone surface) was used as
104 the primary outcome. Three optical machine vision USB3 cameras (acA4096-30uc, Basler AG,
105 Ahrensburg, SH, Germany) were outfitted with c-mount premium lenses (FL-BC3518-9M, Ricoh,
106 Tokyo, Kanto, Japan) (resultant pixel size of 3.45 μm) and focused on the implant-bone interface
107 to collect micromotion measurements at the superior, anterosuperior, and anterior edges of each
108 implant (Figure 5). Micromotion data was extracted from the collected high-resolution digital
109 images using ProAnalyst (Xcitex Inc., Woburn, MA, USA) motion analysis software. All images
110 were collected and stored in Tagged Image File Format (.TIFF). Implant survivability (defined as
111 maximum micromotion of less than 350 μm during the cyclical test), was used as the secondary

112 outcome measure for this study. A limit of 350 μm was utilized, as this was the observed threshold
113 of micromotion before critical macro-failure of the bone or disassociation of the implant occurred.

114 **Statistical Analyses:**

115 A two-way paired repeated measures analysis of variance (ANOVA) was conducted for the
116 dependent variables of neck shaft angle and loading scenario, and a one-way paired repeated
117 measures ANOVA was conducted for the dependent variable of survivability. All statistical
118 analyses were computed using SciPy 1.9.1²³, with the threshold of significance set at $p < 0.05$ and
119 Bonferroni correction with an adjusted alpha level of 0.025 (0.05/2) per two-way test.

120 **Results**

121 At a 145° NSA, all implants experienced significantly lower time-zero micromotions ($P = 0.001$)
122 and survivorship ($P < 0.001$) when compared to the 135° NSA implantations. For all loading
123 scenarios, maximum micromotion was detected on the implant edge that was opposite to the
124 direction of loading. Micromotions detected were significantly higher in the 135° NSA
125 implantations (Table 1)($P = 0.001$) (Figure 6), and the catastrophic failure rate was also
126 significantly higher in the 135° NSA implantations ($P < 0.001$) (135° NSA failures: total $n = 6$ [at
127 load levels: 20%: 0, 40%: 0, 60%: 1, 80%: 3, 100%: 2], 145° NSA failures: total $n = 3$ [at load
128 levels: 20%: 0, 40%: 0, 60%: 1, 80%: 0, 100%: 2]) (Figure 7).

129 **Discussion**

130 The principal objective of this work was to evaluate the comparative biomechanical performance
131 of a metaphyseal filling two-tiered round stemless RSA humeral component implanted at 135°
132 NSA and 145° NSA. We hypothesized that 145° NSA stemless pressfit implants would exhibit
133 better primary fixation and biomechanical survivorship when compared to 135° NSA stemless

134 pressfit implants. Our results identified that increasing NSA from 135° to 145° substantially
135 increased time-zero stemless implant fixation and biomechanical survivorship. Additionally, the
136 results indicated that when stemless humeral components are subjected to cyclical loading, critical
137 implant fixation failure may occur when single-load distractive micromotions are well below the
138 previous referenced limit of 150 µm for successful osseointegration^{2,3,9,14}.

139

140 The osseointegrative potential of porous humeral stemless implants has not yet been thoroughly
141 investigated, and existing studies evaluating the primary fixation of press-fit implants have
142 defaulted to the literature, accepting the 150 µm threshold for osseointegration without fibrous
143 tissue formation^{2,3,9,14}. However, this threshold appears to be relevant to shear or tangential
144 micromotion, commensurate with axially-loaded stemmed implant designs. Indeed, previous
145 reports have indicated that for ideal osseointegration, full contact between the implant and bone
146 should be maintained, and any level of shear or distractive micromotion may potentially negatively
147 influence the success of primary and secondary fixation^{20,22}. The micromotions observed in this
148 work show this threshold of long-term fixation surpassed even at 40% physiological load, which
149 supports the directive of postoperative immobilization to increase the probability of successful
150 long-term fixation.

151

152 Measurement of implant stability is a commonly utilized assessment method when evaluating the
153 osseointegrative potential of different orthopedic implants^{2-4,8,9,17,21}. The use of high-resolution
154 digital tracking methods for the quantification of implant stability (viz micromotion) is becoming
155 more widely utilized^{8,9}. This technique is able evaluate the implant-bone interface during the
156 application of loads that may realistically be experienced postoperatively during activities of daily

157 living^{6,7,16,25}. Although the use of Linear Variable Digital Transformers (LVDTs) has been
158 commonly utilized in the experimental evaluation of shoulder implants², it has previously been
159 found that LVDT methods may overreport implant-bone relative motion⁸, so a high-resolution
160 digital tracking system was used.

161

162 Given the interface changes that were observed due to the loading states simulated, it is logical to
163 postulate that loading of this nature this may be an impediment to osseous integration and may
164 contribute to early migration of subsidence if it were to occur postoperatively. When interpreting
165 the telemetrized implant data available, there are only a limited number of activities that
166 maintained load magnitudes of less than 40% of the physiological boundary load (53% body-
167 weight), and those activities of daily living (ADLs) identified as “safe” were limited to
168 physiotherapist-assisted external rotation motions (in 1/1 patient(s)) and controlled unweighted 90°
169 abduction motions (in 4/17 patient(s))⁶ (Figure 8). It is therefore reasonable to postulate that
170 immobilization during the first four to six weeks after surgery may serve to decrease implant-bone
171 micromotion, thereby increasing the potential for bone on-growth with resultant increased long-
172 term fixation in stemless humeral implants. However, four to six weeks of sling use may result in
173 increased joint stiffness, which may take longer to resolve. Previous investigations on the effect
174 of modifying NSA have reported comparable results; indicating that lower, more varus, NSAs
175 exhibit lower levels of stability⁵; therefore also supporting the position that when implant stability
176 is of concern, higher neck-shaft angles may improve early implant stability in stemless reverse
177 humeral components⁵. Although both the 135° NSA and 145° NSA cohorts experienced failures,
178 it is important to note that the conservative loads utilized for this work were intended to represent

179 the worst-case conditions that a shoulder implant might experience postoperatively, before any
180 osseointegration had occurred.

181

182 Increasing humeral component NSA, however, may have important negative implications;
183 including decreased impingement-free range of motion in adduction²⁴, increased risk of scapular
184 notching¹³, increased humeral distalization, and possibly reduced internal/external rotation^{1,13}. As
185 such, it is important to consider all these factors when selecting an appropriate NSA. When using
186 a traditional stemmed implant with diaphyseal or meta-diaphyseal fixation, the effect of NSA on
187 primary implant stability is likely less pronounced.

188

189 Implant fixation has frequently been studied in the shoulder, however, most studies have focused
190 on glenoid components²; as such, there are limited protocols currently available for the evaluation
191 of humeral component implant performance. In a clinical setting, humeral implants are subjected
192 to a wide range of loading⁶, and hence, it is reasonable to postulate that testing should include a
193 comprehensive protocol. Most recently, studies have employed cyclical loading protocols to better
194 mimic the early performance of uncemented devices^{4,7,10}; a strategy that was also employed herein.
195 Additionally, due to the diverse array of loading states that are experienced by the shoulder
196 postoperatively, this study utilized a novel loading protocol that was designed to examine the
197 fixation of implants using an increasingly aggressive loading protocol. This was important, as this
198 study also aimed to assess the survivability of humeral implants during loading that best attempted
199 to mimic the physiological state.

200

201 As discussed, one of the outcome measures leveraged in this work was distractive micromotion
202 magnitude. This metric is most commonly associated with osseointegration, as bony ingrowth is
203 generally more successful when implant micromotion is limited^{2,3,9,14}. However, existing literature
204 rarely differentiates between tangential (shear) and orthogonal (distractive) micromotion. In fact,
205 to the authors' knowledge, there are no studies that examine the influence of cyclical loading on
206 the osseointegration of surfaces resisting load in the distractive direction. As it has been proposed
207 that the mechanism of implant-bone distractive fixation is dependent on the osseointegrated
208 surface area and level of osseointegration¹⁹, this would imply that when the level of
209 osseointegration is negligible, any loads resulting in distractive micromotions would not be
210 resisted in the orthogonal direction by adhesion phenomena¹¹, and hence osseous ingrowth in the
211 distractive direction may be compromised by comparatively small micromotion magnitudes. This
212 is noteworthy, as for implant geometries that rely on fixation to a primarily cancellous bone
213 foundation, eccentric loading is known to cause "lift-off" and hence analyses of fixation in these
214 constructs requires assessment of implant micromotion orthogonal to the interface. Previous finite
215 element studies for the evaluation of micromotion in humeral implants found the primary mode of
216 micromotion at the interface to be distractive micromotion for a similar implant geometry
217 investigated⁷. Hence, distractive micromotion was utilized as the outcome measure of this work,
218 but 150 µm was not purposed as a hard limit as knowledge on the relevance of that value is
219 disputed. The experimental approaches employed herein have also been widely employed for
220 tibial and glenoid implants^{2,14,21}.

221

222 There are limitations with the present study. Primarily, boundary loading limits were established
223 using in-vivo telemetritized data for anatomic implants. This is noteworthy, as reversed implants

224 are likely to experience lower magnitudes of articular force at potentially higher eccentricities due
225 to the medialized center of rotation and increased deltoid moment arm¹⁵. However, for the
226 purposes of this work, a conservative approach using larger magnitude loading was used as
227 telemetrized data for RSA implants is not yet available⁵. This evaluation also focused on time-
228 zero (directly after implantation) implant behaviors. As trabecular bone is a mechanoresponsive
229 material and press-fit implants rely on osseointegration for fixation, stability during the
230 postoperative rehabilitation period may differ in a clinical setting. Lastly, this evaluation only
231 investigated one design of stemless RSA humeral implant. Future works should assess additional
232 implant designs with a large variation in fixation geometry to provide a more thorough evaluation
233 of the effect of neck shaft angle.

234 Conclusion

235 Neck shaft angle in stemless reverse humeral components is a modifiable intra-operative
236 parameter that significantly effects the time-zero stability and early survivorship of the stemless
237 reverse humeral component implant design tested. The results demonstrate that a metaphyseal
238 filling round two-tiered stemless implant inserted at an NSA of 145° exhibits better primary
239 stability than when inserted at 135° during simulated early postoperative physiological loading
240 scenarios. It is suggested, therefore, with conditions of poorer humeral bone quality, that a higher,
241 more valgus, neck shaft angle may be considered to maximize time zero stemless implant fixation.
242 Alternatively, sling immobilization to limit provocative activities of daily living in the early
243 postoperative period will decrease undesirable bone-implant micromotions.

244 References:

- 245 1. Arenas-Miquelez A, Murphy RJ, Rosa A, Caironi D, Zumstein MA. Impact of humeral and
246 glenoid component variations on range of motion in reverse geometry total shoulder

- 247 arthroplasty: a standardized computer model study. *J Shoulder Elbow Surg.*
248 2021;30(4):763–771. doi:10.1016/j.jse.2020.07.026
- 249 2. ASTM. ASTM F2028-17 Standard Test Methods for Dynamic Evaluation of Glenoid
250 Loosening or Disassociation. 2018;1–15. doi:10.1520/F2028-17.
- 251 3. Bonnevialle N, Geais L, Müller JH, Berhouet J. Effect of RSA glenoid baseplate central
252 fixation on micromotion and bone stress. *JSES Int.* 2020;4(4):979–986.
253 doi:10.1016/j.jseint.2020.07.004
- 254 4. Chen RE, Knapp E, Qiu B, Miniaci A, Awad HA, Voloshin I. Biomechanical comparison
255 of stemless humeral components in total shoulder arthroplasty. *Seminars Arthroplasty:*
256 *JSES*. 2021;1–9. Adoi:10.1053/j.sart.2021.08.003
- 257 5. Cunningham DE, Spangenberg GW, Langohr GDG, Athwal GS, Johnson JA. Stemless
258 Reverse Humeral Component Neck Shaft Angle has an Influence on Initial Fixation. *J*
259 *Shoulder Elbow Surg.* 2023; doi:10.1016/j.jse.2023.06.035
- 260 6. Damm P, Dymke J. Orthoload Database . Jul. Wolff Inst. 2021 [cited 2021 Jul 26];Available
261 from: <https://orthoload.com/database/>
- 262 7. Favre P, Henderson AD. Prediction of stemless humeral implant micromotion during upper
263 limb activities. *Clin. Biomech.* . 2016;36:46–51. doi:10.1016/j.clinbiomech.2016.05.003
- 264 8. Favre P, Perala S, Vogel P, Fucentese SF, Goff JR, Gerber C, et al. In vitro assessments of
265 reverse glenoid stability using displacement gages are misleading - Recommendations for
266 accurate measurements of interface micromotion. *Clin. Biomech.* . 2011;26(9):917–922.
267 doi:10.1016/j.clinbiomech.2011.05.002
- 268 9. Favre P, Seebek J, Thistleton PAE, Obrist M, Steffens JG, Hopkins AR, et al. In vitro
269 initial stability of a stemless humeral implant. *Clin. Biomech.* . 2016;32:113–117.

- 270 doi:10.1016/j.clinbiomech.2015.12.004
- 271 10. Freitag T, Kutzner KP, Bieger R, Reichel H, Ignatius A, Dürselen L. Biomechanics of a
272 cemented short stem: a comparative in vitro study regarding primary stability and maximum
273 fracture load. Arch. Orthop. Trauma Surg. . 2021;141(10):1797–1806. doi:10.1007/s00402-
274 021-03843-x
- 275 11. Gao X, Fraulob M, Haïat G. Biomechanical behaviours of the bone-implant interface: A
276 review. J. R. Soc. Interface. 2019;16(156). doi:10.1098/rsif.2019.0259
- 277 12. Gobezie R, Shishani Y, Lederman E, Denard PJ. Can a functional difference be detected in
278 reverse arthroplasty with 135° versus 155° prosthesis for the treatment of rotator cuff
279 arthropathy: a prospective randomized study. J Shoulder Elbow Surg. 2019;28(5):813–818.
280 doi:10.1016/j.jse.2018.11.064
- 281 13. Jeon BK, Panchal KA, Ji JH, Xin YZ, Park SR, Kim JH, et al. Combined effect of change
282 in humeral neck-shaft angle and retroversion on shoulder range of motion in reverse total
283 shoulder arthroplasty - A simulation study. Clin. Biomech. . 2016;31:12–19.
284 doi:10.1016/j.clinbiomech.2015.06.022
- 285 14. Kohli N, Stoddart JC, van Arkel RJ. The limit of tolerable micromotion for implant
286 osseointegration: a systematic review. Sci. Rep. . 2021;11(1):1–11. 5doi:10.1038/s41598-
287 021-90142-5
- 288 15. Langohr GD. Fundamentals of the Biomechanical Characteristics Related to the Loading of
289 Reverse Total Shoulder Arthroplasty Implants and the Development of a Wear Simulation
290 Strategy . Available from:
291 https://ir.lib.uwo.ca/etd/3436/?utm_source=ir.lib.uwo.ca%2Fetd%2F3436&utm_medium=
292 PDF&utm_campaign=PDFCoverPages

- 293 16. Masjedi M, Johnson GR. Glenohumeral contact forces in reversed anatomy shoulder
294 replacement. *J. Biomech.* . 2010;43(13):2493–2500. doi:10.1016/j.jbiomech.2010.05.024
- 295 17. Quental C, Folgado J, Comenda M, Monteiro J, Sarmento M. Primary stability analysis of
296 stemless shoulder implants. *Med. Eng. Phys.* 2020;81:22–29.
297 doi:10.1016/j.medengphy.2020.04.009
- 298 18. Razfar N. Finite Element Modeling of the Proximal Humerus to Compare Stemless , Short
299 and Standard Stem Humeral Components of Varying Material Stiffness for Shoulder
300 Arthroplasty . Univ. West. Ontario - Electron. Thesis Diss. Repos. 2014;2431. Available
301 from: <https://ir.lib.uwo.ca/etd/2431>
- 302 19. Rønold HJ, Ellingsen JE. The use of a coin shaped implant for direct in situ measurement
303 of attachment strength for osseointegrating biomaterial surfaces. *Biomaterials.*
304 2002;23(10):2201–2209. doi:10.1016/S0142-9612(01)00353-2
- 305 20. Sánchez E, Schilling C, Grupp TM, Giurea A, Wyers C, van den Bergh J, et al. The effect
306 of different interference fits on the primary fixation of a cementless femoral component
307 during experimental testing. *J. Mech. Behav. Biomed. Mater.* 2021;113(September 2020).
308 doi:10.1016/j.jmbbm.2020.104189
- 309 21. Suárez DR, Nerkens W, Valstar ER, Rozing PM, van Keulen F. Interface micromotions
310 increase with less-conforming cementless glenoid components. *J Shoulder Elbow
311 Surg*2012;21(4):474–482. doi:10.1016/j.jse.2011.03.008
- 312 22. Viceconti M, Brusi G, Pancanti A, Cristofolini L. Primary stability of an anatomical
313 cementless hip stem: A statistical analysis. *J. Biomech.* 2006;39(7):1169–1179.
314 doi:10.1016/j.jbiomech.2005.03.024
- 315 23. Virtanen P, Gommers R, Oliphant TE, Haberland M, Reddy T, Cournapeau D, et al. SciPy

- 316 1.0: fundamental algorithms for scientific computing in Python. *Nat. Methods.*
317 2020;17(3):261–272. doi:10.1038/s41592-019-0686-2
- 318 24. Werner BS, Chaoui J, Walch G. The influence of humeral neck shaft angle and glenoid
319 lateralization on range of motion in reverse shoulder arthroplasty. *J Shoulder Elbow Surg.*
320 2017;26(10):1726–1731. doi:10.1016/j.jse.2017.03.032
- 321 25. Zimmerman WF, Miller MA, Cleary RJ, Izant TH, Mann KA. Damage in total knee
322 replacements from mechanical overload. *J. Biomech.* . 2016;49(10):2068–2075.
323 doi:10.1016/j.jbiomech.2016.05.014

324 **Figures:**

325 Figure 1: NSA Cut Guide: Depicting the intermedullary diaphyseal referencing guide and 135°
326 NSA cut-guide attachment.

327 Figure 2: A custom three-dimensional loading apparatus used to apply physiological loads to a
328 stemless humeral RSA implant. For the purposes of the figure, a 135° NSA specimen has been
329 positioned for loading. Loads were applied using an array of (5) pneumatic actuators, which
330 articulated pistons with polished force pads. Combines of loads on each actuator applied resolved
331 physiological loads to the 42 mm ball bearing, which was utilized as a proxy for the glenosphere
332 component of the RTSA. The potted humeral specimen was positioned at using a custom adaptable
333 potting fixture to facilitate a static boundary condition during loading.

334 Figure 3: Scatter plots of relevant OrthoLoad⁶ load vectors relative to the local resection coordinate
335 system. (A) represents a summary of all vector tails orthogonal to the resection plane, whereas (B)
336 indicates the relevant loads' eccentricities relative to the resection plane. The Superior,
337 Anterosuperior, and Anterior simulated loads are indicated by the red arrows and dots. All loading

338 directions were evaluated at the most aggressive eccentricity experienced in order to simulate the
339 most challenging loading profile to implant stability.

340 Figure 4: Boundary loads representing 95% of loading scenarios available on the OrthoLoad⁶
341 database. The humerus represented in the figure is a left side specimen resected at 135° NSA.

342 Figure 5: A high-resolution image of the implant-bone interface on the superior periphery (position
343 depicted by red arrow on the resection view in the top left) of the stemless humeral implant with
344 respect to the humeral resection plane on a 135° NSA model. White markings on the bone (A) and
345 implant (B) served as tracking points during micromotion measurement. The Anterosuperior and
346 Anterior regions of interest relative to the resection plane view are indicated by yellow arrows.

347 Figure 6: Micromotions developed in stemless reversed implants based on loading magnitude,
348 NSA, and loading direction. Where an implant did not survive during a trial, it was given a
349 micromotion of N/A and is not shown on the plot.

350 Figure 7: Survivability of stemless reversed implants based on NSA and cycles survived at
351 increasing load magnitudes. The above plot [A] shows the number of specimens surviving at each
352 loading case, whereas the below plot [B] shows a representation of the cyclical loading at
353 increasing magnitudes. Please note that the plot in [B] is a representation of the cyclical loading,
354 and in actuality, each specimen underwent a total of 90 cycles at each load level.

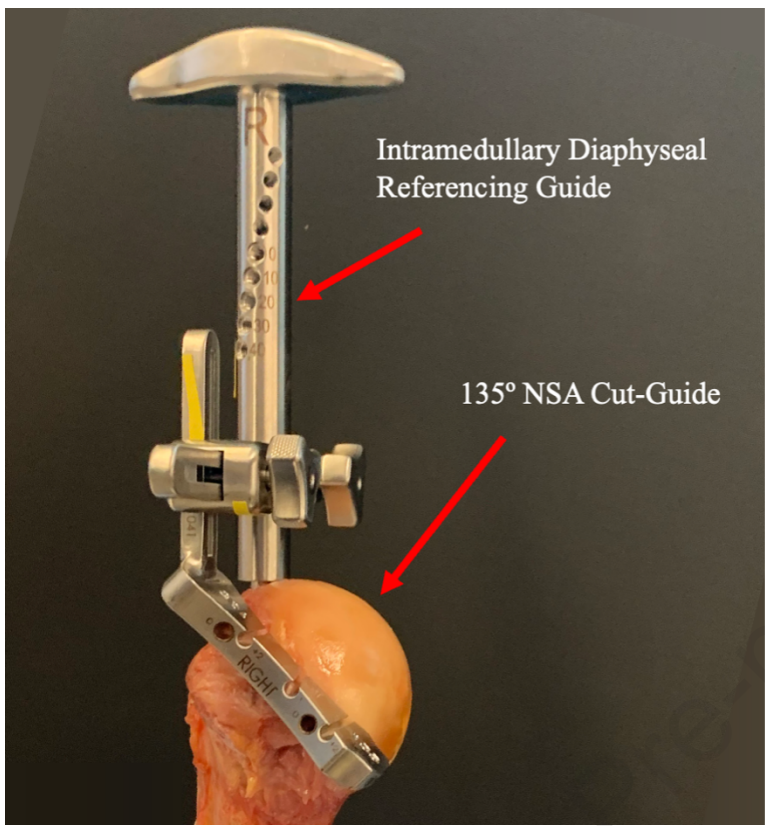
355 Figure 8: A 3D plot of the proximal humerus, showing all relevant OrthoLoad⁶ activities used in
356 the calculation of boundary loading limits in vector format. All black arrows represent ADLs that
357 exceed the 40% physiological load survivorship limit determined by the study. The red arrows
358 show the ADLs that were below the 40% limit. Only No-Weight Abduction and External Rotation

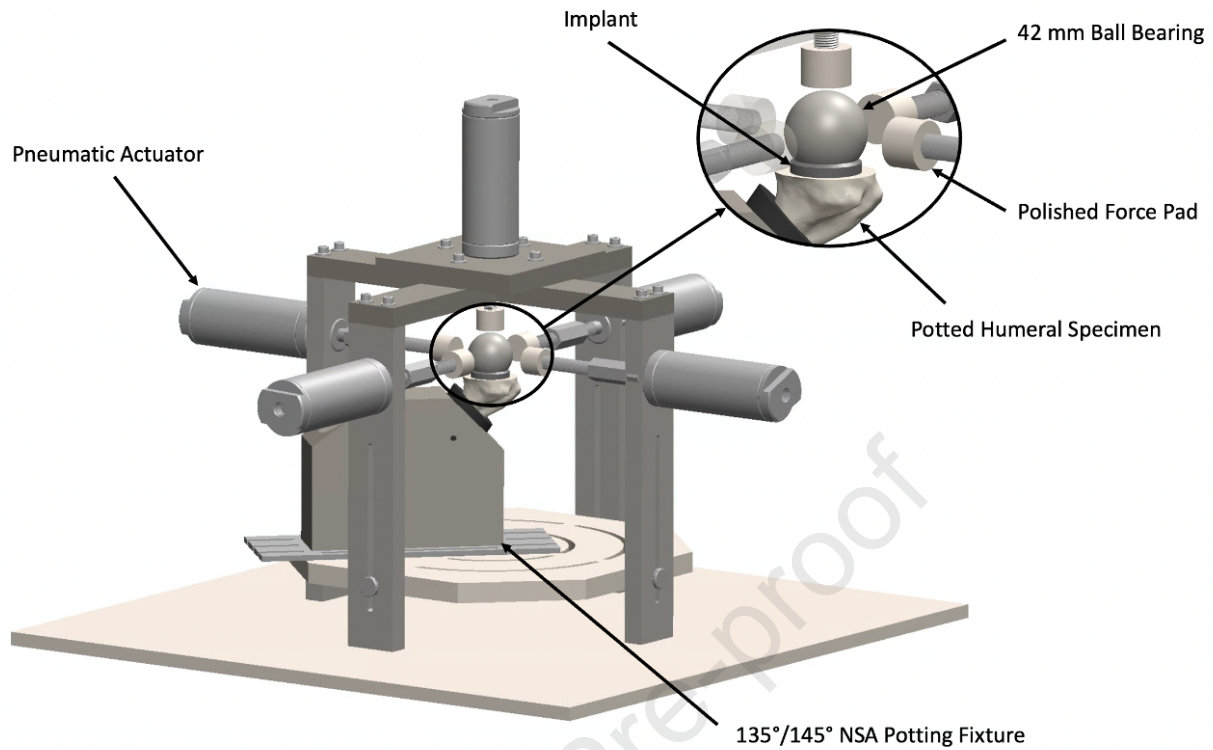
359 in 90° Elbow Flexion, supported by a physiotherapist were determined as “safe” activities in a few
360 of the patients.

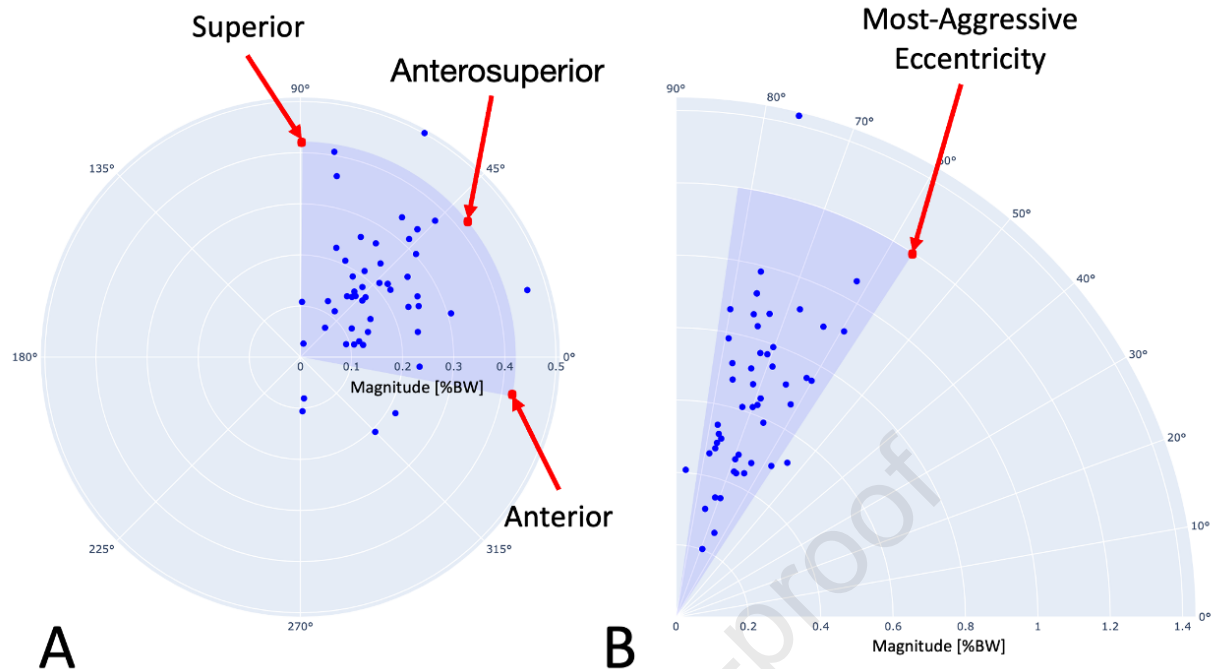
361 **Tables:**

362 Table 1: Micromotion Data during Increasing Cyclical Load Tests

	Direction	20%	40%	60%	80%	100%
135°	Average	11 ± 4	35 ± 27	118 ± 93	100 ± 9	153 ± NaN
	Superior	16 ± 7	40 ± 18	138 ± 99	53 ± 16	74 ± NaN
	Anterior	10 ± 6	74 ± 103	80 ± 72	181 ± 205	None Survived.
145°	Average	8 ± 6	23 ± 19	36 ± 27	69 ± 39	134 ± 114
	Superior	10 ± 3	25 ± 22	45 ± 47	85 ± 76	139 ± 100
	Anterior	6 ± 2	31 ± 27	37 ± 29	122 ± 76	234 ± 128







Physiological Boundary Forces

